AIMS Mathematics, 9(3): 5877−5885.
DOI: 10.3934/math.2024286
Received: 25 November 2023
Revised: 07 January 2024
Accepted: 25 January 2024
Published: 31 January 2024

http://www.aimspress.com/journal/Math

Communication

Sound reduction of a panel-cavity system with a chaotically vibrating boundary

Yiuyin Lee*

Department of Architecture and Civil Engineering, City University of Hong Kong, Kowloon Tong, Kowloon, Hong Kong

* **Correspondence:** Email: bcraylee@cityu.edu.hk; Tel: +85234427609; Fax: +85234420427.

Abstract: Here, I was the first to investigate the sound reduction of a chaotically vibrating curved panel with/without a cavity. A sound reduction formula was obtained by combining the homogeneous wave equation and nonlinear structural governing equation. The chaotic and nonlinear sound radiations were computed from the multi-mode coupled formulations using a numerical integration method. The results obtained from the proposed method and classical harmonic balance method were generally in reasonable agreement. A modal convergence study was also performed to check the proposed method. The effects of chaotic vibration on the sound reduction of a curved panel with/without a cavity were studied in detail.

Keywords: chaotic vibration; nonlinear structural dynamics; vibro-acoustics; sound reduction; panel-cavity system
Mathematics Subject Classification: 65M99, 65P99, 37M05

1. Introduction

Over the past twenty years, not more than 40 research papers about nonlinear structural-acoustics have been presented (e.g., [1−3]). Most of these studies employed classic methods (such as harmonic balance method and multiple scales method) to solve various problems about a nonlinearly vibrating panel backed by a cavity. Only periodic vibration and acoustic responses were generated from these methods. On the other hand, there have been some research works about chaotic panel vibration. For example, Pourtakdoust and Fazelzadeh [4] investigated the effect of structural damping on the chaotic behavior of a panel subject to supersonic flow. The nonlinear governing equations were developed using the concept of Von Karman's large deflection and the first order piston theory. Chandiramani et al. [5] presented a study about the

nonlinear vibrations of a composite panel subjected to uniform edge compression and a high-supersonic coplanar flow. The third-order piston theory aerodynamics, the effects of in-plane edge restraints, small initial geometric imperfections, transverse shear deformation, and transverse normal stress were considered in their model. Liu et al. [6] considered circular sandwich panels designed with aluminum as core material, steel and Al-Al-based high entropy alloy (Al-based HEA) as the surface board materials, respectively. They developed a finite element model to study the nonlinear and chaotic responses and the influence of small changes in thickness and inherent properties. The aforementioned works focused on the structural responses in various panel models only. Among those works, Ng [7] was the only one to propose using acoustic excitations to generate chaotic vibration responses. However, his work did not focus on any results about sound radiation. Particularly, research works about the effects of chaotic vibration on the acoustic properties of a panel are extremely limited. Three of them are mentioned here. The work in [8] addressed the chaotic phenomena in a vibro-acoustic system. The conditions about triggering the non-chaotic responses to chaotic responses were presented. It focused on the structural vibration responses only and did not mention any acoustic properties. The other work in [9] addressed a study about the sound radiation of a curved panel. It did not consider a cavity backing the curved panel and the effects of chaotic vibration on the sound reduction. Lee [10] adopted an approach of panel impedance and perforation impedance to derive the sound absorption of a chaotically vibrating curved perforated panel. Its focus and formulation were totally different from that in this paper. In practice, the chaotic vibrations of curved panels would be induced by large excitations. That can affect their sound reduction performances. Here, I was the first to investigate the sound reduction of a chaotically vibrating curved panel with/without a cavity.

2. Theoretical formulation

Figure 1 shows two curved panel cases (one is with cavity; the other one is without cavity). In the case with cavity, one of the boundaries is a chaotically or nonlinearly vibrating panel. The homogeneous wave equation, the acoustic modal decomposition equation [8−10] and boundary conditions are given by

$$\nabla^2 P_m - \frac{1}{C_a^2}\frac{\partial^2 P_m}{\partial t^2} = 0; \tag{1}$$

$$P_m = \sum_{J=1}^{\bar{J}} P_{mJ}(t)\varphi_J(x,y,z) \tag{2}$$

$$\frac{\partial P_m}{\partial z} = -\rho_o \frac{\partial^2 w_m}{\partial t^2} \text{ at } z = 0; \tag{3}$$

$$\frac{\partial P_Q}{\partial z} = -\rho_o \frac{\partial^2 w_o}{\partial t^2} \text{ at } z = c \tag{4}$$

where P_m is the acoustic pressure induced by the m^{th} mode vibrations of the curved panel and source panel; ϕ_m is the structural mode (i.e., $\sin(m\pi x/a)$); φ_J is the J^{th} acoustic mode shape (i.e., $\cos(l_x\pi x/a)$ $\cos(l_y\pi y/b)$ $\cos(l_z\pi z/c)$, l_x, l_y, and l_z are the acoustic mode numbers, a and b are the panel width and length, and c is the cavity depth; $\bar{J}$ is the number of acoustic mode used; C_a is the speed of sound; w_o and w_m are the excitation source displacement and curved panel displacement, which are expressed in the forms of $w_o = A_o(t)\phi_1(x,y)$, $w_m = A_m(t)\,\phi_m(x,y)$, $\partial^2 A_o/\partial t^2 = \lambda g \sin(\omega t)$ and A_m is the modal displacement; ω is the excitation frequency; and λ is the dimensionless excitation parameter and g is the gravity of $9.81 ms^{-2}$.

By applying the boundary conditions (i.e., Eqs (3) and (4)) to Eq (1), the acoustic pressure induced by the vibrations of the curved panel and source panel is given by

$$P_m(t,x,y,z) = \sum_{J=1}^{\bar{J}} \left[\frac{\rho_o \gamma_{mJ}}{\left[(k)^2-(k_J)^2\right]\alpha_{JJ}} \frac{\mathrm{d}^2 A_m}{\mathrm{d}t^2} - \frac{\rho_o \gamma_{1J}}{\left[(k)^2-(k_J)^2\right]\alpha_{JJ}} \lambda g sin(\omega t) \right] \varphi_J(x,y,z) \quad (5)$$

where k is the wave number of the excitation frequency; k_J is the wave number of the J^{th} acoustic mode; $\alpha_{JJ} = \int_V \varphi_J \varphi_J dv$; $\gamma_{mJ} = \int_S \phi_m \varphi_J ds$; ϕ_m is the m^{th} vibration mode shape function, V is the cavity volume and S is the corresponding panel surface.

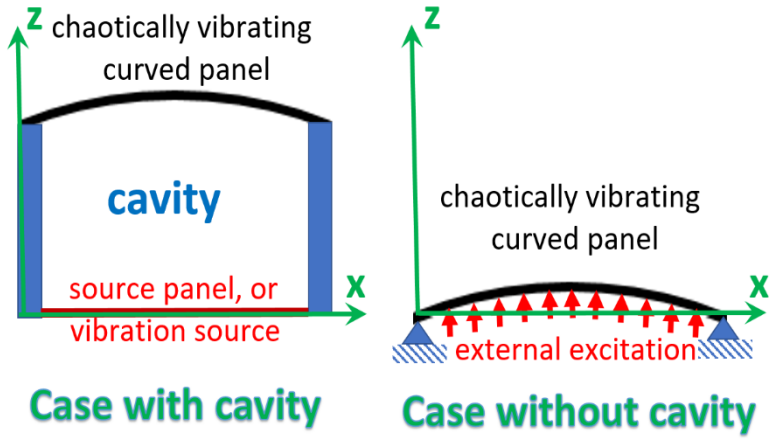

Figure 1. Curved panel cases with/without cavity.

The governing equation of the curved panel vibration and the structural modal decomposition equations are given as follows [8−10].

$$\rho_p \frac{\mathrm{d}^2 w}{\mathrm{d}t^2} + \xi \frac{\mathrm{d}w}{\mathrm{d}t} + EI \frac{\mathrm{d}^4 w}{\mathrm{d}x^4} = \frac{Ebh}{a} \frac{d^2(w+\overline{w})}{dx^2} \int_0^a \left(\frac{\mathrm{d}w}{\mathrm{d}x} \frac{\mathrm{d}\overline{w}}{\mathrm{d}x} + \frac{1}{2} \left(\frac{\mathrm{d}\overline{w}}{\mathrm{d}x} \right)^2 \right) dx = F(t) \quad (6)$$

$$w = \sum_{m=1}^{\bar{m}} A_m \phi_m \quad (7)$$

where w is the transverse displacement; $\overline{w}$ is the pre-set initial displacement profile ($\overline{w}$=$A_o$sin($\pi x/a$)); $\overline{m}$ is the number of structural modes used; E is the Young's modulus; I is the section property; ρ_p is the panel surface density; ξ is the panel damping coefficient; a, b, and h are the panel width, length and thickness, respectively; and $F(t)$ is the uniform external force or the acoustic pressure force acting on the panel. Note that according to [8−10], the "beam like" curved panel was adopted and the flexural modes along the y direction were ignored. Consider the substitution of Eq (7) into (6) and then preform the modal decomposition procedure. The governing equation of the modal nonlinear panel vibration is given by

$$\rho_p \Lambda_{11}^{00} \frac{\mathrm{d}^2 A_1}{\mathrm{d}t^2} + \rho_p \xi \omega \Lambda_{11}^{00} \frac{\mathrm{d}A_1}{\mathrm{d}t} + EI \Lambda_{11}^{40} A_1 \quad - \frac{Ebh}{a} \Lambda_{11}^{11} (A_0)^2 A_1 \quad - \frac{Ebh}{2a} \Lambda_{11}^{20} \left[\Lambda_{11}^{11} (A_1)^3 + \Lambda_{22}^{11} A_1 (A_2)^2 + \Lambda_{33}^{11} A_1 (A_3)^2 \right] \quad - \frac{Ebh}{2a} \Lambda_{11}^{20} A_o \left[3\Lambda_{11}^{11} (A_1)^2 + \Lambda_{22}^{11} (A_2)^2 + \Lambda_{33}^{11} (A_3)^2 \right]$$

$$= \rho_o \sum_{J=1}^{\bar{J}} \frac{\gamma_{1J}}{\left[(k)^2-(k_J)^2\right]\alpha_{JJ}} \frac{\mathrm{d}^2 A_1}{\mathrm{d}t^2} - \rho_o \sum_{J=1}^{\bar{J}} \frac{(\gamma_{1J})^2}{\left[(k)^2-(k_J)^2\right]\alpha_{JJ}} \lambda g \sin(\omega t) \quad \textit{for case with cavity,}$$

$$\textit{or} \quad = \int_0^a \lambda \rho_p g \sin(\omega t)\, \phi_1 dx \quad \textit{for case without cavity} \quad (8)$$

$$\rho_p \Lambda_{22}^{00} \frac{\mathrm{d}^2 A_1}{\mathrm{d}t^2} + \rho_p \xi \omega \Lambda_{22}^{00} \frac{\mathrm{d}A_1}{\mathrm{d}t} + EI \Lambda_{22}^{40} A_1$$

$$- \frac{Ebh}{2a} \left[2\Lambda_{11}^{11} \Lambda_{22}^{20} A_0 A_1 A_2 + \Lambda_{11}^{11} \Lambda_{22}^{20} A_2 (A_1)^2 + \Lambda_{22}^{11} \Lambda_{22}^{20} (A_2)^3 + \Lambda_{33}^{11} \Lambda_{22}^{20} A_2 (A_3)^2 \right]$$

$$= \rho_o \sum_{J=1}^{\bar{J}} \frac{\gamma_{1J}}{\left[(k)^2-(k_J)^2\right]\alpha_{JJ}} \frac{\mathrm{d}^2 A_2}{\mathrm{d}t^2} - \rho_o \sum_{J=1}^{\bar{J}} \frac{(\gamma_{1J})^2}{\left[(k)^2-(k_J)^2\right]\alpha_{JJ}} \lambda g \sin(\omega t) \quad \textit{for case with cavity,}$$

$$\textit{or} \quad = \int_0^a \lambda \rho_p g \sin(\omega t)\, \phi_2 dx \quad \textit{for case without cavity} \quad (9)$$

$$\rho_p \Lambda_{33}^{00} \frac{\mathrm{d}^2 A_1}{\mathrm{d}t^2} + \rho_p \xi \omega \Lambda_{33}^{00} \frac{\mathrm{d}A_1}{\mathrm{d}t} + EI\Lambda_{33}^{40} A_1$$

$$-\frac{Ebh}{2a}\left[2\Lambda_{11}^{11}\Lambda_{33}^{20} A_0 A_1 A_3 + \Lambda_{11}^{11}\Lambda_{33}^{20} A_3 (A_1)^2 + \Lambda_{22}^{11}\Lambda_{33}^{20} A_3 (A_2)^2 + \Lambda_{33}^{11}\Lambda_{33}^{20} (A_3)^3\right]$$

$$= \rho_o \sum_{J=1}^{\bar{J}} \frac{\gamma_{1J}}{\left[(k)^2-(k_J)^2\right]\alpha_{JJ}} \frac{\mathrm{d}^2 A_3}{\mathrm{d}t^2} - \rho_o \sum_{J=1}^{\bar{J}} \frac{(\gamma_{1J})^2}{\left[(k)^2-(k_J)^2\right]\alpha_{JJ}} \lambda g \sin(\omega t) \quad \textit{for case with cavity,}$$

$$\textit{or} \quad = \int_0^a \lambda \rho_p g \sin(\omega t)\, \phi_3 dx \quad \textit{for case without cavity} \quad (10)$$

where $\Lambda_{mn}^{00} = \int_0^a \phi_m \phi_n \mathrm{d}x$; $\Lambda_{mn}^{20} = \int_0^a \frac{\mathrm{d}^2\phi_m}{\mathrm{d}x^2} \phi_n \mathrm{d}x$; $\Lambda_{mn}^{40} = \int_0^a \frac{\mathrm{d}^4\phi_m}{\mathrm{d}x^4} \phi_n dx$; $\Lambda_{mn}^{11} = \int_0^a \frac{\mathrm{d}\phi_m}{\mathrm{d}x} \frac{\mathrm{d}\phi_n}{\mathrm{d}x} dx$ (m,n =1,2,3). Note that the equations for three only 3 structural modes are adopted. In the next section, the convergence study showed that this three mode approach is accurate enough.

The above coupled modal differential equations can be solved using the Runge-Kutta time domain numerical integration [8−10]. Hence, the overall root-mean square modal velocity at the steady state can be obtained. The sound reduction is defined as

$$Sound\ Reduction = \Phi = -10 \log\left[\frac{\sum_{m=1}^{3} \sigma_m \langle \dot{A}_m \rangle^2}{(\lambda g/\omega)^2}\right] \quad (11)$$

where σ_m is the sound radiation efficiency of the m^{th} mode; $\dot{A}_m$ is the modal velocity response; <·> is the root square mean value. Note that $\sum_{m=1}^{3} \sigma_m \langle \dot{A}_m \rangle^2$ is the total normalized sound energy; $(\lambda g/\omega)^2$ is the total normalized energy acting on the panel; $\langle \dot{A}_m \rangle^2$ is the normalized modal vibration energy; and $\sigma_m \langle \dot{A}_m \rangle^2$ is the normalized modal sound energy [9].

3. Results and discussion

In Table 1, the physical dimensions and material properties of the metal panel are 400mm × 300mm × 2mm, Young's modulus = 7×10^{10} N/m^2, Poisson's ratio = 0.3, damping ratio = 0.02, and panel density = 2700 kg/m^3. Table 1 shows the mode convergence for various excitation magnitudes. The pre-set center deflection is 4mm. The cavity depth is 300mm. The first 16 acoustic modes are used. It can be seen that the contribution of the 2$^{\text{nd}}$ anti-symmetric mode is very minimal, and thus the 3 mode approximation is accurate enough. Note that the sound radiation efficiencies of the anti-symmetric modes are much lower than those of the symmetric modes. Therefore, the contribution of the 1$^{\text{st}}$ anti-symmetric mode is significantly lower than that of the 2$^{\text{nd}}$ symmetric mode. Figure 2 shows the comparison between the phase plots obtained from the numerical integration method and classical harmonic balance method [3]. It is a case of no cavity, no initial center deflection (i.e., flat panel), and undamped free vibration (the initial displacement = 1.4 × panel thickness). The physical dimensions of the panel are 500mm × 400mm × 2mm. The other panel properties are the same as those in Table 1. The two sets of results agree reasonably well with each other.

Table 1. Modal sound radiation contribution.

	1st sym. mode	1st anti-sym. mode	2nd sym. Mode	2nd anti-sym. mode
λ = 40	98.34%	0.01%	1.65%	0.00%
= 20	99.40%	0.01%	0.59%	0.00%
= 10	97.86%	0.01%	2.12%	0.00%
= 5	97.85%	0.01%	2.14%	0.00%

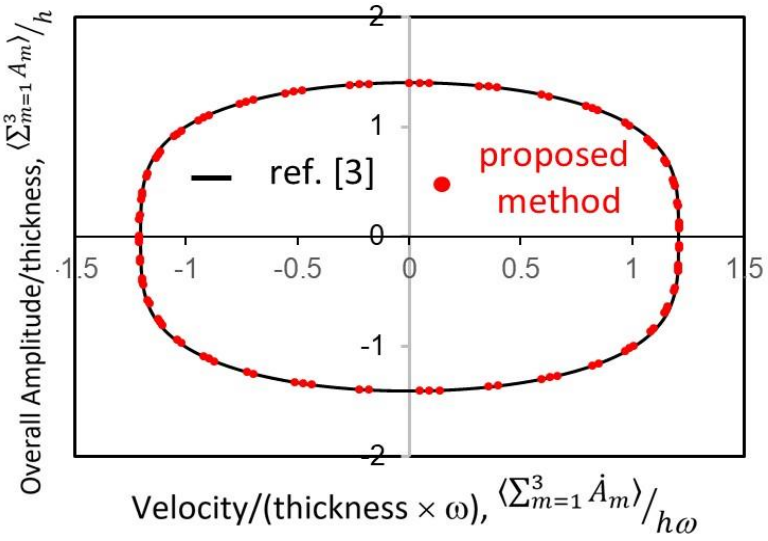

Figure 2. Comparison between the phase plot results.

Figures 3 and 6 show the sound reductions in the cases with/without cavity for various excitation magnitudes. The panel properties in these two figures are the same as those in Table 1, except the pre-set center deflection = 10mm and damping ratio = 0.01. In Figure 3, the chaotic responses, which exist when λ = 100 (the red line), deteriorate the sound reduction performance for the entire frequency range except the frequency range near the primary resonant dip (f = 340 to 360 Hz). The two-phase plots (f =80 Hz and 360 Hz) show the chaotic properties. Figures 4 and 5 show the corresponding time histories. Obviously, the responses are non-periodic and non-repeatable so that they are classified as chaotic response. In the green line, blue line and black line cases, only nearly linear and nonlinear responses can be generated. It can be seen that the higher the excitation magnitude is, the smaller the primary resonant dips are induced. Interestingly, the higher the excitation magnitude is, the bigger the high order nonlinear dips are induced.

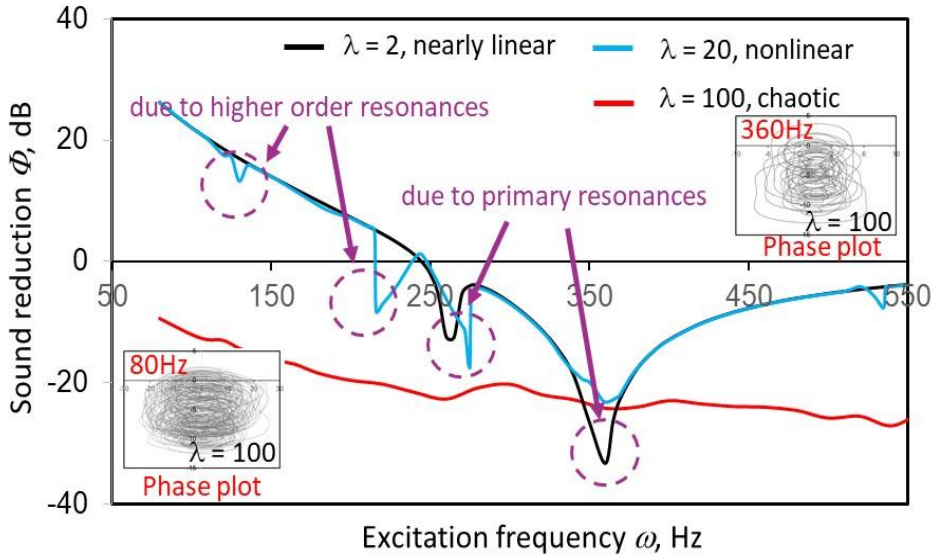

Figure 3. Sound reduction of the case without cavity.

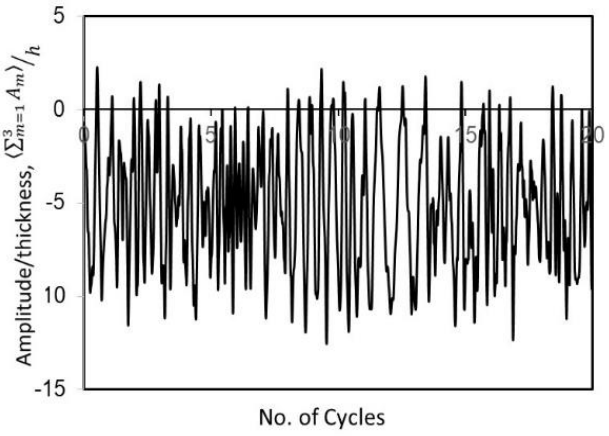

Figure 4. Time history of the phase plot in Figure 3 (80Hz).

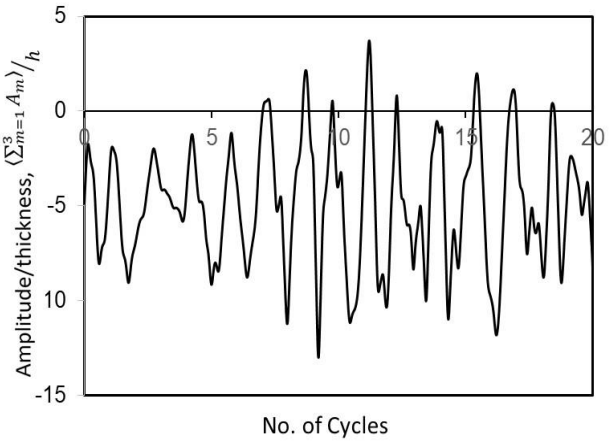

Figure 5. Time history of the phase plot in Figure 3 (360Hz).

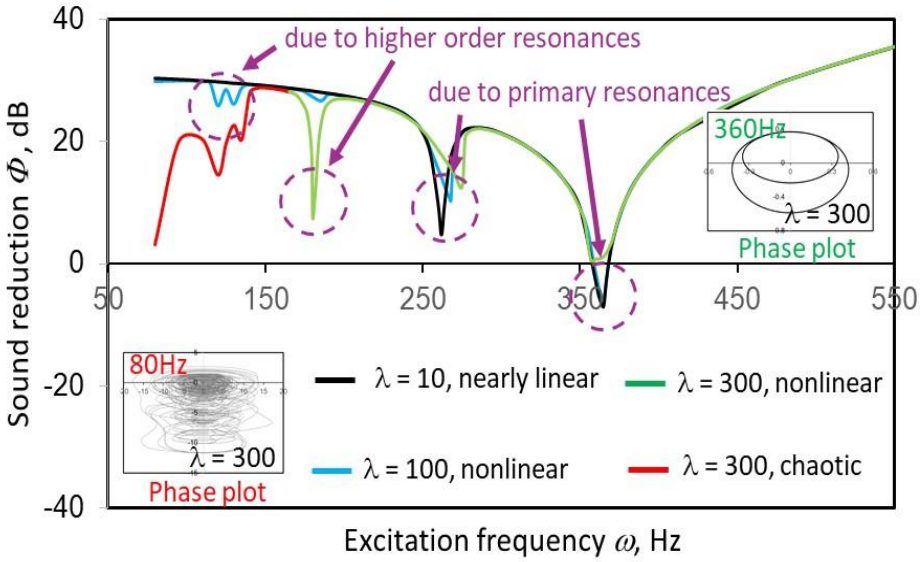

Figure 6. Sound reduction of the case without cavity.

In Figure 6, the chaotic responses (the red portion), which only exist when the excitation magnitude is very high ($\lambda = 300$) and excitation frequency is very low ($f < 150$ Hz), deteriorate the sound reduction performance. The sound performance at that frequency range is abruptly lower (the red portion). The comparison between the cases with/without cavity in Figures 3 and 6 shows that it requires much higher excitation level to induce the chaotic vibrations ($\lambda = 100$ in Figure 3 and $\lambda = 300$ in Figure 6). It is because the cavity acts as a "cushion" to strength the system. The phase plot (f =80 Hz, $\lambda = 300$) shows the chaotic properties, while the other phase plot (f =360 Hz, $\lambda = 300$) shows the nonlinear multi-frequency properties. Figures 7 and 8 show the corresponding time histories. Note that the responses in Figure 7 are chaotic, and the responses in Figure 8 are periodic. Similar to the green line, blue line and black line cases in Figure 3, the higher the excitation magnitude is, the smaller the primary resonant dips are induced; the higher the excitation magnitude is, the bigger the high order nonlinear dips are induced. Figure 9 shows the corresponding vibration amplitude curves, at which the well-known jump phenomenon can be observed. There is no jump phenomenon in Figure 6. This is because the dominant mode at the orange portion in Figure 9 is anti-symmetric. As aforementioned, the radiation efficiencies of anti-symmetric modes are very minimal. Thus, that nonlinear portion in Figure 9 does not exist on the sound reduction curve in Figure 6. When the cavity depth is bigger, the "cushion" effect is also bigger and thus the vibration amplitude is smaller. It can be seen that the curve of $c = 300$mm is the lowest and the vibration responses are nearly linear (no chaotic vibration is found in that case). In the case of $c = 200$mm, the vibration responses are less nonlinear than those in the case of $c = 100$mm, and the frequency range of chaotic vibration is also narrower.

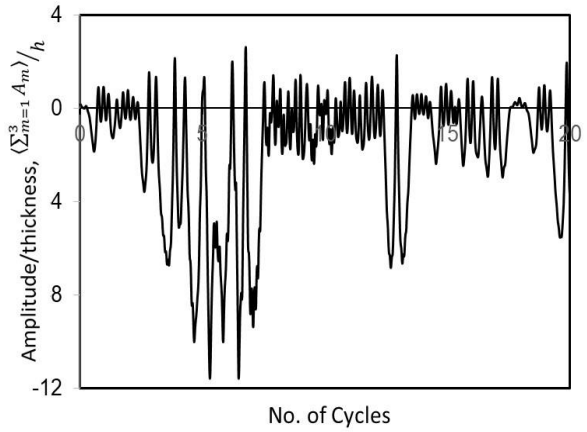

Figure 7. Time history of the phase plot in Figure 6 (80Hz).

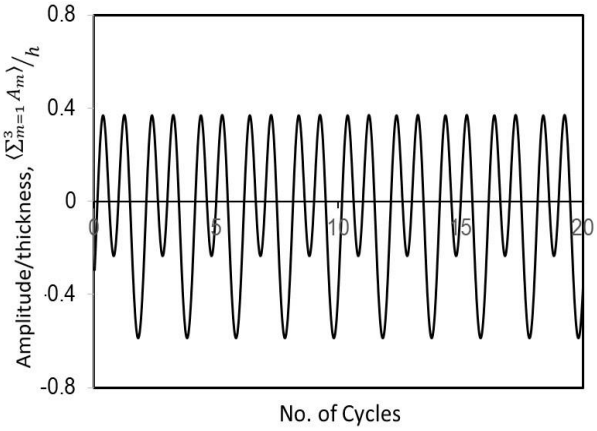

Figure 8. Time history of the phase plot in Figure 6 (80Hz).

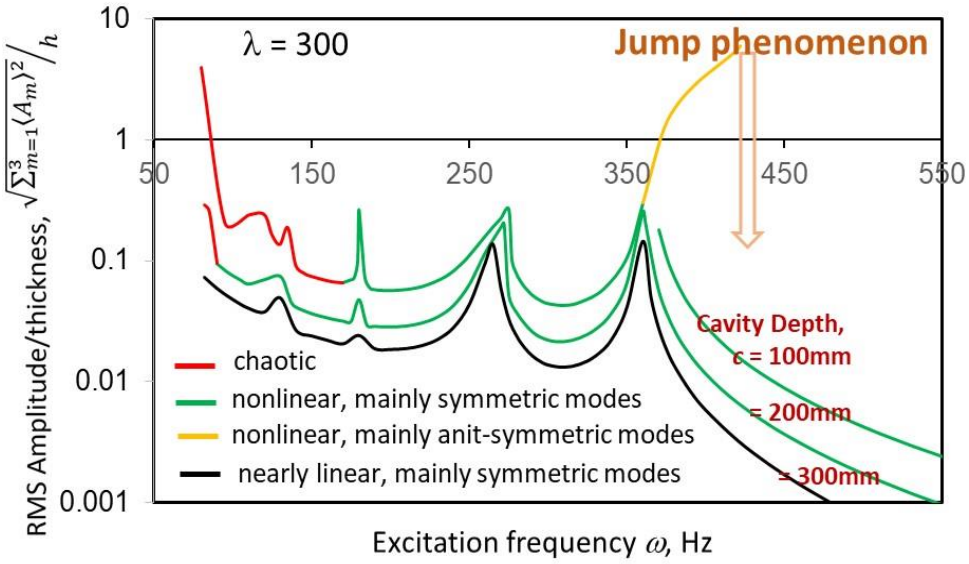

Figure 9. Vibration amplitude of the case with cavity.

4. Conclusions

The effects of chaotic and nonlinear vibrations on the sound reduction of a curved panel have been studied for the cases with/without cavity. The present solution agrees reasonably well with that obtained from the classical harmonic balance method. The results show that: 1) The case with cavity needs much higher excitation magnitude to trigger chaotic vibrations. It is because the cavity acts as a "cushion" to strength the system. When the cavity depth or volume is bigger, the "cushion" effect is also bigger and thus the vibration amplitude is smaller; 2) the chaotic vibrations would deteriorate the sound reduction performance for the entire frequency range except the frequency range near the primary resonant dip; 3) there is no jump phenomenon at the sound reduction curve because the radiation efficiencies of anti-symmetric modes are very low; 4) the higher the excitation magnitude is, the smaller the primary resonant dips are induced, and the bigger the high order nonlinear dips are induced.

Use of AI tools declaration

The author declares that they have not used Artificial Intelligence (AI) tools in the creation of this article.

Conflict of interest

The author declares that they have no competing interests in this paper.

References

1. M. Sadri, D. Younesian, Nonlinear harmonic vibration analysis of a plate-cavity system, *Nonlinear Dynam.*, **74** (2013), 1267–1279. https://doi.org/10.1007/s11071-013-1039-9
2. F. S. Anvariyeh, M. M. Jalili, A. R. Fotuhi, Nonlinear vibration analysis of a circular plate-cavity system, *J. Braz. Soc. Mech. Sci. Eng.*, **41** (2019), 66. https://doi.org/10.1007/s40430-019-1565-6
3. Y. Y. Lee, Structural-acoustic coupling effect on the nonlinear natural frequency of a rectangular box with one flexible plate, *Appl. Acoust.*, **63** (2002), 1157−1175. https://doi.org/10.1016/s0003-682x(02)00033-6
4. S. H. Pourtakdoust, S. A. Fazelzadeh, Effect of structural damping on chaotic behavior of nonlinear panel flutter, *Iran. J. Sci. Technol.*, **27** (2003), 453−467. Available from: https://ijstm.shirazu.ac.ir/article_978.html.
5. N. K. Chandiramani, R. H. Plaut, L. I. Librescu, Nonperiodic flutter of a buckled composite panel, *Sadhana-Acad. P. Eng. Sci.*, **20** (1995), 671−689. https://doi.org/10.1007/ bf02823212
6. X. M. Liu, J. T. Fan, X. S. Liu, G. Li, Nonlinear vibration of Al-Al based high entropy alloy circular sandwich panel, *AIP Adv.*, **9** (2019), 035351. https://doi.org/10.1063/1.5086914
7. C. F. Ng, Testing techniques for chaotic vibration of buckled aircraft structures, *P. I. Mech. Eng.-G Aer.*, **210** (1996), 281−290. https://doi.org/10.1243/pime_proc_1996_210_371_02
8. Y. Y. Lee, Chaotic phenomena and nonlinear responses in a vibroacoustic system, *Complexity*, 2018, 7076150. https://doi.org/10.1155/2018/7076150
9. Y. Y. Lee, C. K. Hui, W. Z. Lu, E. W. M. Lee, The low frequency sound radiation of a chaotically vibrating curved beam/panel, *Int. J. Nonlin. Sci. Num.*, **10** (2009), 1159−1166. Available from: https://www.degruyter.com/document/doi/10.1515/IJNSNS.2009.10.9.1159/html?lang=en.
10. Y. Y. Lee, Chaotic vibration and perforation effects on the sound absorption of a nonlinear curved panel absorber, *Mathematics*, **11** (2023), 3178. https://doi.org/10.3390/math11143178

© 2024 the Author(s), licensee AIMS Press. This is an open access article distributed under the terms of the Creative Commons Attribution License (http://creativecommons.org/licenses/by/4.0)